Coupling between second-order mode in dielectric waveguide and fundamental mode in long range surface plasmon waveguide

Yunxiang Li, Fang Liu*, Yidong Huang, Boyu Fan, Ruiyuan Wan

Department of Electronic Engineering, Tsinghua University, Beijing 100084, China

ARTICLE INFO

ABSTRACT

The coupling between long range surface plasmon polariton (LRSPP) waveguide mode and dielectric waveguide second-order mode has been studied theoretically and experimentally. It is demonstrated that an almost pure TM-polarized second-order mode of dielectric waveguide is excited efficiently by the LRSPP fundamental mode. The proposed hybrid coupler inspires a new way for generating high-order waveguide modes, especially the high-order SPP waveguide modes, which is promising for mode division multiplexing, bio/chemical sensing, photonic circuits and other optical applications.

© 2012 Elsevier B.V. All rights reserved.

1. Introduction

Surface plasmon polariton (SPP) is a transverse magnetic surface wave that propagates along a metal-dielectric interface [1]. It has drawn more attention nowadays due to its unique features and potential applications in the field of integrated optical circuits, sensing, and nano-lithography [2–5].

Recently, the hybrid couplings between various SPP modes and dielectric waveguide modes have been proposed and studied [6–17]. The extremely high coupling efficiency (> 99%) between LRSPP waveguide (LRSPP-WG) fundamental mode and TM dielectric waveguide (D-WG) fundamental mode has been demonstrated theoretically and experimentally [6], which can be used for a high performance polarization splitter with pure TM output. Besides, the SRSPP waveguide mode, which cannot be easily excited by traditional methods due to its anti-symmetric mode field distribution, can be effectively excited by this kind of hybrid coupler [7]. Meanwhile, because the coupling efficiency of the hybrid coupler is closely related to the refractive index of the medium surrounding the metal, a compact refractive index sensor with high sensitivity can be realized [8].

In this paper, we demonstrate theoretically and experimentally a hybrid coupler with higher-order coupling. The coupling phenomenon between fundamental mode of LRSPP-WG and TM-polarized second-order mode of D-WG has been observed. In this hybrid coupler, a pure TM-polarized second-order mode of D-WG could be excited by the LRSPP-WG efficiently. This provides us one way for realizing the mode multiplexing/demultiplexing in mode-division multiplexing, which is promising to satisfy the exponential growth of data capacity required in today's transmission system. Compared with current methods based on the free spatial optics [18,19], the hybrid coupler proposed here has the advantage of simple structure, easy integration, and high performances. Furthermore, it is expected that the high-order LRSPP-WG mode could also be excited by the D-WG mode as long as properly designing the hybrid coupler. These high-order waveguide modes, especially the high-order LRSPP-WG modes, have potential in bio/chemical sensing, integrated photonic circuits, and other optical applications.

2. Structure and simulation result

Fig. 1(a) shows the schematic structure of the hybrid coupler, which is composed of an Au waveguide (yellow) and a SiN_x waveguide (gray) surrounded by the SiO_2. The whole structure is designed for telecommunication wavelength ($\lambda_0 = 1.55\ \mu m$). The cross section with detailed parameters is also shown. The finite element method was applied to calculate the eigenmodes of individual D-WG, LRSPP-WG and the coupler, from which the electromagnetic field and propagation constants can be obtained. According to normal mode expansion method, any supported mode in the hybrid coupler can be expressed in terms of a linear superposition of the eigenmodes supported by the coupler [21].

$$H(x,y,z) = \sum_j a_j H_j(x,y)e^{i\beta_j z} \tag{1}$$

$$E(x,y,z) = \sum_j a_j E_j(x,y)e^{i\beta_j z} \tag{2}$$

* Corresponding author.
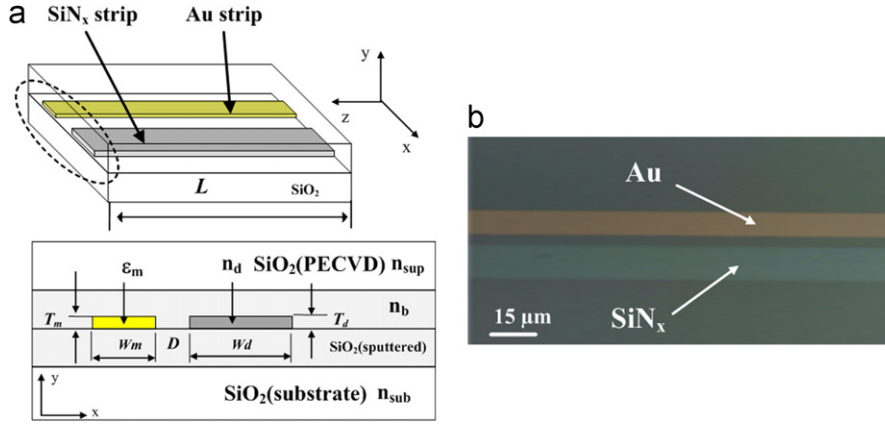   *E-mail address:* liu_fang@mail.tsinghua.edu.cn (F. Liu).

Fig. 1. (a) Schematic structure of the hybrid coupler composed of an Au strip (yellow) and a SiN$_x$ strip (gray). The inset is the cross section of the coupler in the x–y plane . Here, $W_d=15$ μm, $T_d=40$ nm, $W_m=8$ μm, $T_m=11$ nm, $D=6$ μm, $n_d=1.87$, $n_{sup}=1.448$, $n_b=1.453$, $n_{sub}=1.446$, $\varepsilon_m=-132+12.66i$, $\lambda_0=1.55$ μm (b) the microscopical photo of the hybrid coupler. (For interpretation of the references to color in this figure legend, the reader is referred to the web version of this article.)

where the subscript j is the number of the eigenmode, H_i and E_i are the magnetic field and electronic field of the eigenmodes, and β_i and α_i are the corresponding propagation constant and modes constant respectively. Here the light is coupled into the LRSPP-WG at the beginning of the coupler. So the electromagnetic field of the coupler when $z=0$ can be expressed as

$$H(x,y,0)=\sum_j a_j H_j(x,y)e^{i\beta_j z}=H_{LRSPP} \tag{3}$$

$$E(x,y,0)=\sum_j a_j E_j(x,y)e^{i\beta_j z}=E_{LRSPP} \tag{4}$$

where H_{LRSPP} and E_{LRSPP} are the electromagnetic field of the individual LRSPP-WG eigenmode. And the modes constant can be derived from

$$a_j=\frac{1}{2}\int \left(E_{LRSPP}\times H_j^*\right)\cdot\hat{z}dxdy, \tag{5}$$

where all the modes have been normalized,

$$\frac{1}{2}\int \left(E_j\times H_j^*\right)\cdot\hat{z}dxdy=1, \tag{6}$$

Hence the coupling phenomenon can be well revealed by using above equations and the calculated results with the finite element method. And the analysis is based on the parameters of the actual fabricated coupler. Here only TM-polarized mode should be considered because the coupling only occurs for TM modes [20,21].

Fig. 2 shows effective refractive indices (n_{eff}, the real part of the propagation constant) of both D-WG fundamental and second-order eigenmodes with different widths of the SiN$_x$ waveguide as well as the n_{eff} of LRSPP-WG fundamental mode with fixed width of $W_m=8$ μm. As shown in Fig. 2, when the D-WG gets wider, its ability for field confinement gets stronger resulting in the increase of the n_{eff}. When W_d is about 5 μm, the n_{eff} of the D-WG fundamental mode is close to that of the LRSPP-WG fundamental mode. The high efficient coupling between these two modes have been observed and discussed in another paper [6]. When the W_d increases, the second-order mode could be supported by the SiN$_x$ waveguide and its n_{eff} gets closer to that of the LRSPP-WG fundamental mode, while the n_{eff} of the D-WG fundamental mode is far away from that of the LRSPP-WG mode. In this case, the effective coupling tends to occur between the LRSPP-WG fundamental mode and the D-WG second-order mode rather than the D-WG fundamental mode.
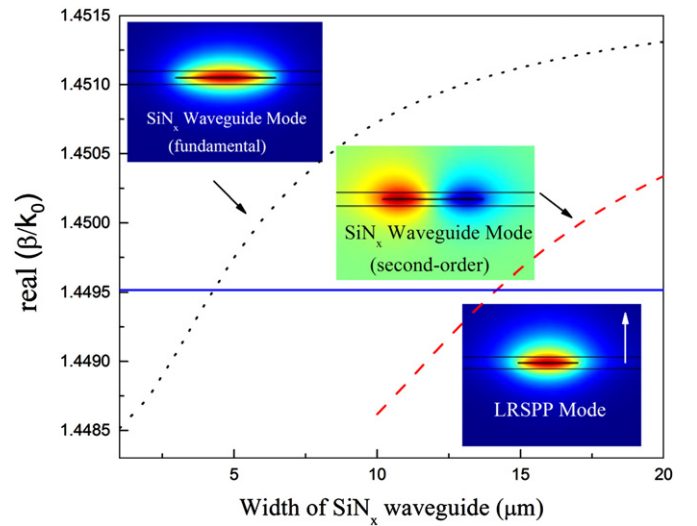

Fig. 2. The real part of the propagation constants of dielectric waveguide modes and LRSPP waveguide mode vs the width of the SiN$_x$ waveguide. The $|E_y|$ distributions of the dielectric waveguide modes ($W_d=15$ μm) and the LRSPP waveguide mode ($W_m=8$ μm) are in the insets.

For the case of $W_d=15$ μm, the hybrid coupler structure has two TM coupled eigenmodes as shown in Fig. 3(a) and (b). The even and odd eigenmode respectively results from the in-phase and opposite-phase coupling between LRSPP-WG fundamental mode and dielectric waveguide second-order mode. Further, the coupling characteristics can be easily analyzed with these two eigenmodes of the coupler [21]. The energy transfer between the two arms of the coupler is shown in Fig. 3(c). A LRSPP-WG fundamental mode is assumed as the input of the coupler and the energy transfers gradually from the Au arm to the SiN$_x$ arm along the propagation direction. At the coupling length L_c, almost all the energy is guided by the SiN$_x$ waveguide in the form of the D-WG second-order mode.

Actually, besides the eigenmode A and B, another TM-polarized eigenmode can also be guided by the hybrid coupler when $W_d=15$ μm, which is almost the same as the fundamental mode guided by the SiN$_x$ waveguide shown in Fig. 2. This means there is no coupling between the LRSPP-WG mode and the D-WG fundamental mode, which results from the large mismatch of effective refractive index of these two modes and small field overlap.
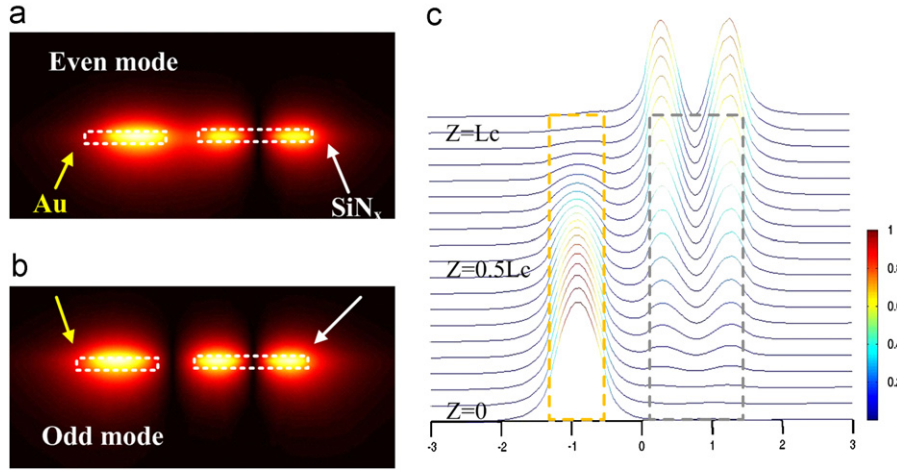
Fig. 3. For the hybrid coupler ($W_d = 15$ μm) at $\lambda_0 = 1.55$ μm, (a) the amplitude of $|E_y|$ of two TM eigenmodes (b) the power distribution along the propagation direction z with TM-polarized input light at the LRSPP waveguide.
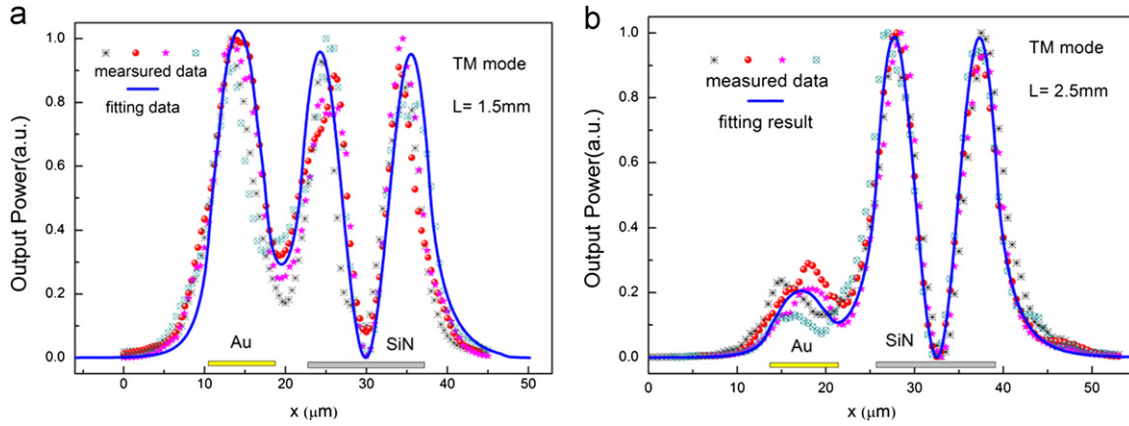

Fig. 4. Output power profiles along the x axis of four samples for the coupler length (a) $L = 1.5$ mm, (b) $L = 2.5$ mm. The blue lines are fitting result of the measured data, which is a linear combination of the LRSPP waveguide fundamental eigenmode and dielectric waveguide second-order eigenmode. (For interpretation of the references to color in this figure legend, the reader is referred to the web version of this article.)

3. Fabrication and measurement

Fig. 1(b) shows the microscopical photo of the hybrid coupler. To fabricate this hybrid coupler, a Si wafer covered by a 15 μm-thick SiO_2 layer ($n_{sub} = 1.446$) is selected as the substrate. On the substrate, a 1 μm-thick SiO_2 ($n_b = 1.453$) layer and a $T_d = 32$ nm-thick SiN_x ($n_d = 1.871$) layer are deposited by sputtering and plasma-enhanced chemical-vapor deposition (PECVD), respectively. After UV lithography, reactive ion etching and removing the photoresist, the SiN_x waveguides with width of $W_d = 15$ μm is realized. Next the cover-lithography, Au magnetic sputtering and lifting-off process had been applied to fabricate Au strips of $W_m = 8$ μm wide and $T_m = 12$ nm thick. Here, the Au strip is carefully set to be parallel to the SiN_x waveguide by accurate cover-lithography process, and the distance D of these two arms is 6 μm. Then another 1 μm-thick SiO_2 ($n_b = 1.453$) layer is sputtered over the couplers for the sake of maintaining the identical refractive index of medium around the LRSPP waveguide. At last, a 9 μm-thick SiO_2 ($n_{sup} = 1.448$) is deposited by PECVD as a covering layer.

After the fabrication process, the hybrid coupler is cut into several samples with different length L and measured. The measurement system includes a laser, a polarization controller, a pair of tapered lens fibers, a fiber alignment system and a power meter. With the help of the fiber alignment system, the tapered lens fibers are accurately aligned to the input/output ends of the coupler for effective energy injection/extraction.

The TM-polarized light at the wavelength of 1.55 μm is applied on the LRSPP waveguide through the input fiber. The output power profile along the x axis is obtained by horizontally scanning the output end of the coupler. Fig. 4(a) and (b) represent the output power profile when the length of the coupler is 1.5 mm and 2.5 mm, respectively. It illustrates that there are two output power peaks with almost the same shape and height on the SiN_x waveguide side, which should be owe to the D-WG second-order mode. And the close-to-zero deep between the two peaks indicates that little fundamental mode is guided by the SiN_x waveguide and a nearly pure second-order mode has been exited in the SiN_x waveguide. The solid lines in Fig. 4 are the fitting curves of the measured data, which is a linear combination of field profile of the LRSPP-WG fundamental eigenmode and D-WG second-order eigenmode. The energy transfer is defined as follows:

$$energy \ transfer = \frac{\tau_{D-WG}}{\tau_{D-WG} + \tau_{LRSPP-WG}} \tag{7}$$

where τ_{D-WG} and $\tau_{LRSPP-WG}$ is the integration of the LRSPP-WG fundamental eigenmode and D-WG second-order eigenmode obtained from the fitting result, respectively.

For the case of $L = 1.5$ mm, only about 60% of the energy has been coupled to the dielectric waveguide. When $L = 2.5$ mm,
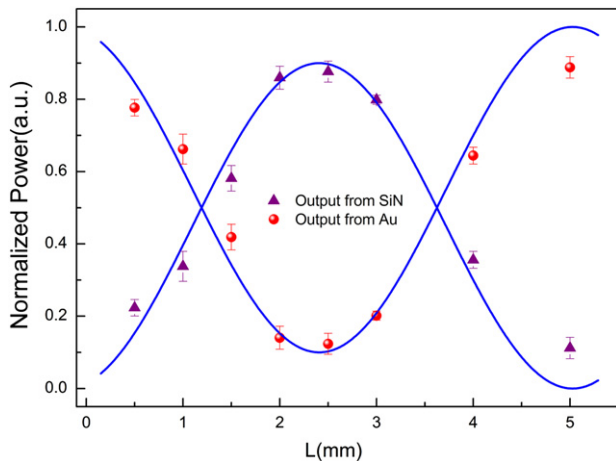
Fig. 5. The output power from the SiN$_x$ arm (purple triangle) and the Au arm (red dot) vs. the coupler length L. Here the TM-polarized light at $\lambda=1.55$ μm is applied at the Au arm. (For interpretation of the references to color in this figure legend, the reader is referred to the web version of this article.)

almost 85% of the energy has been transferred from the LRSPP-WG fundamental mode into the D-WG second-order mode

Furthermore, the hybrid couplers at different lengths ($L=0.5$, 1, 1.5, 2, 2.5, 3, 4, 5 mm) are measured and the normalized output power from the Au arm (red dot) and the SiN$_x$ arm (purple triangle) is shown in Fig. 5. A periodic energy exchange occurs between the two waveguides of the coupler, which is an obvious sign of coupling phenomenon. And the coupling length is around $L_c=2.5$ mm with the coupling efficiency up to 85%. The coupling efficiency of the hybrid coupler here is not so high due to the imperfect match of n_{eff} between the LRSPP-WG fundamental mode and the D-WG second-order mode when $W_d=15$ μm as shown in Fig. 2. The coupling efficiency can be improved by carefully designing the coupler structure, for example, setting the width of SiN$_x$ waveguide around 14 μm for nearly perfect match between two different modes.

4. Conclusions

In conclusion, the coupling between the fundamental mode of LRSPP-WG and TM higher-order mode of D-WG has been studied theoretically and experimentally. The coupling efficiency high up to 85% is observed. Based on this coupler, an effective mode filter can be realized. Assuming a mixing mode containing both the fundamental and second-order mode is excited initially at the

dielectric arm of the hybrid coupler, the energy of the second-order mode in dielectric arm will completely transfer into the LRSPP arm while the nearly pure fundamental mode remains in the dielectric arm. Besides, an extremely pure dielectric waveguide second-order mode can be provided by this hybrid coupler. By carefully designing the parameters of the coupler, the coupling between any mode (not only the fundamental mode but also the high-order mode) of the dielectric waveguide or the LRSPP waveguide can be realized, which provides one way to generate high-order mode in D/LRSPP-WG and is possible to be used for various applications [18,19].

References

[1] P. Berini, Physical Review B 61 (2000) 10484.
[2] P. Berini, Adv. Opt, Photon 1 (2009) 484.
[3] Z. Liu, Q Wei, X Zhang, Nano Letters 5 (2005) 957.
[4] Yongqi Fu, Xiuli Zhou, Plasmonics 5 (2010) 287.
[5] T. Nikolajsen, K. Leosson, S.I. Bozhevolnyi, Applied Physics Letters 85 (2004) 5833.
[6] F. Liu, R. Wan, Y. Li, Y. Huang, Y. Miura, D. Ohnishi, J. Peng, Applied Physics Letters 95 (2009) 091104.
[7] R. Wan, F.Y. Huang, S. Hu, B. Fan, Y. Miura, D Ohnishi, Y Li, H Li, Y Xia, Applied Physics Letters 97 (2010) 141105.
[8] F. Liu, R. Wan, Y. Huang, J. Peng, Optics Letters 34 (2009) 2697.
[9] Y. Song, J. Wang, M. Yan, M. Qiu, Optics Express 18 (2010) 13173.
[10] Q. Li, M. Qiu, Optics Express 18 (2010) 15531.
[11] Y. Song, J. Wang, M. Yan, M. Qiu, Journal of Optics 13 (2011) 075002.
[12] S. Choi, J.Y. Kim, Optics Communications 285 (2012) 3735.
[13] Y. Fang, Z. Chen, L. Chen, K. He, Z. Han, Z. Wang, Optics Express 19 (2011) 2562.
[14] F. Lou, Z. Wang, D. Dai, L. Thylen, L. Wosinski, Applied Physics Letters 100 (2012) 241105.
[15] J. Shin, M. Kwon, S. Shin, Optics Communication 284 (2011) 3522.
[16] R. Mote, H. Chu, P. Bai, E. Li, Optics Communication 285 (2012) 3709.
[17] C. Delacour, S. Blaize, P. Grosse, J.M. Fedeli, A. Bruyant, R. Salas-Montiel, G. Lerondel, A. Chelnokov, Nano Letters 10 (2010) 2922.
[18] C. Koebele, M. Salsi, D. Sperti, P. Tran, P. Brindel, H. Mardoyan, S. Bigo, A. Boutin, F. Verluise, P. Sillard, M. Astruc, L. Provost, F. Cerou, G. Charlet, Optics Express 19 (2011) 16595.
[19] N. Hanzawa, K. Saitoh, T. Sakamoto, T. Matsui, S. Tomita, and M. Koshiba, Optical Fiber Communication Conference (Optical Society of America, (2011), Paper OWA4.
[20] F. Liu, Y. Rao, Y. Huang, W. Zhang, J. Peng, Applied Physics Letters 90 (2007) 141101.
[21] F. Liu, Y. Li, R. Wan, Y. Huang, X. Feng, W. Zhang, J. Lightw., Technol 29 (2011) 1265.